Energetic wave equation for modelling diffuse sound fields. I: corridor case

Hugo Dujourdy, Baptiste Pialot, Thomas Toulemonde, Jean-Dominique Polack

Energetic wave equation for modelling diffuse sound fields. I: corridor case

Hugo Dujourdy[1,2,3], Baptiste Pialot[1,2],
Thomas Toulemonde,[3] Jean-Dominique Polack[1,2],

[1] Sorbonne Universités, UPMC Univ Paris 6, UMR 7190,
Institut Jean le Rond d'Alembert, F-75005 Paris, France,
[2] CNRS, UMR 7190, Institut Jean le Rond d'Alembert, F-75005 Paris, France,
[3] Impédance S.A.S., 80 domaine de Montvoisin, 91400 Gometz-la-ville, France.
h.dujourdy@impedance.fr

Abstract

By revisiting the relationships between energy density and sound intensity, this paper presents an energetic wave equation adapted for long room such as corridors. This linear, second-order, hyperbolic equation depends on few parameters such as mean free path, absorption and scattering coefficients. We solve it by a finite difference in time domain technique and compare the results with in situ measurements carried out with a SoundField microphone to find appropriate values of the model parameters by an adjustment procedure.

Keywords: *architectural acoustic, energy density, wave equation, scattering coefficient, room acoustic modelling, in situ measurement, SoundField microphone.*

1 Introduction

When characterizing the acoustics of closed spaces, to-day's practitioners adapt their prediction tools to the case at hand. Basically two types of tools are available, depending on the amount of details they are looking for. For simple spaces, where only reverberation matters, Sabine's theory and its variants are well adapted: they give quick and realistic results. For complex spaces, such as concert venues, ray-tracing techniques are mostly used, as a comprehensive documentation of the acoustics is required. However, ray-tracing suffers from two main shortcomings: it is not adapted to low frequencies where the modal structure of the sound field dominates (small rooms); and it needs supplementing by a statistical model of some sort in order to accurately model the reverberant tails of the responses [1, 2, 3], otherwise predictions are unrealistic [4, 5].

A commonly used statistical model to improve the reverberant tails is the introduction of scattering, with reflections based on Lambert's law. The model has been popularized by Kutruff in the 70's [6], and several variants of it, including radiosity models [7], have been developed. Common to them is to consider exchanges of acoustical energy between boundary elements, and to iterate the exchanges until stable energy decays are obtained everywhere in the space. They give realistic results, but their strong assumptions limit their applicability [8].

A simpler statistical model, based on a diffusion equation, was proposed by Ollendorff [9] and developed by Picaut and his collaborators [10, 11]. It introduces diffusion coefficients within the volume of the space, leading to non uniform reverberant fields decaying with distance from the source, as are observed in disproportionate spaces where one dimension is very different from the others. Therefore, the diffusion model can be viewed as an extension of Sabine's model [12]. However, attempts to relate the volume diffusion coefficient to wall scattering have been unsuccessful so far [13].

The present work is an attempt to overcome this limitation of the Ollendorff-Picaut diffusion model. Like the diffusion model, it roots in Morse and Feshback's textbook [14]. But instead of considering energy conservation only, and supplement it with some sort of state equation linking sound energy to sound intensity by means of the scattering coefficient, it makes use of the full stress-energy tensor [15] to obtain a second equation between energy and intensity (Sec. 2). We solve this set of equations in Sec. 3 under the form of a linear, second order, hyperbolic, differential

equation focused on the energy density with a finite difference time domain (FDTD) method. We chose an explicit and fast-computing, one-dimensional algorithm. The boundary conditions are mixed. Space and time discretization steps, stability and consistence are presented.

An energy and momentum balance on the walls permits to introduce the absorption and scattering coefficients. By integrating on the cross-section of the room, we obtain a one-dimensional equation. Consequently, the method is adapted to long rooms such as corridors. In Sec. 4 we validate the model and compare the results with *in situ* measurements. Sec. 5 discusses the results and Sec. 6 concludes the paper.

In the following, we follow the recommendation of Embrechts [16], and use the word "diffusion" to the process within the room. The process on the wall is called "scattering".

2 Theory

We consider the wave equation applied to the velocity potential Ψ defined by $\vec{v} = -\vec{\nabla}\Psi$ and $p = \rho\partial_t\Psi$ where $\vec{v}$ is the particle velocity vector, $\vec{\nabla}$ the gradient operator, ρ the air density, p the sound pressure and where we note ∂_i and ∂_{ii} the first and second derivatives according to coordinate i respectively. We have

$$\frac{1}{c^2}\partial_{tt}\Psi - \Delta\Psi = 0 \tag{1}$$

with Δ the Laplacian operator and c the speed of sound in the medium.

2.1 Energy density conservation

Multiplying Eq. (1) by the first time derivative $\partial_t\Psi$ leads to the conservation of energy to a factor ρ that we neglect in the following:

$$\partial_t\Psi\frac{1}{c^2}\partial_{tt}\Psi - \partial_t\Psi\Delta\Psi = 0$$

Applying Leibnitz formula for linear differential operator products, we successively obtain

$$\begin{aligned}
\partial_t\Psi\frac{1}{c^2}\partial_{tt}\Psi &= \frac{1}{2c^2}\partial_t(|\partial_t\Psi|^2) \\
\partial_t\Psi\Delta\Psi &= \vec{\nabla}\cdot(\partial_t\Psi\vec{\nabla}\Psi) - \vec{\nabla}\partial_t\Psi\cdot\vec{\nabla}\Psi \\
&= \vec{\nabla}\cdot(\partial_t\Psi\vec{\nabla}\Psi) - \frac{1}{2}\partial_t|\vec{\nabla}\Psi|^2
\end{aligned}$$

where $\vec{\nabla}\cdot$ is the divergence operator. Subtracting both lines, we obtain

$$-\vec{\nabla}\cdot(\partial_t\Psi\vec{\nabla}\Psi) + \frac{1}{2}\partial_t(\frac{1}{c^2}|\partial_t\Psi|^2 + |\vec{\nabla}\Psi|^2) = 0 \tag{2}$$

Morse and Feshback [14] defined the energy density E:

$$E = \frac{\rho}{2}(\frac{1}{c^2}|\partial_t\Psi|^2 + |\vec{\nabla}\Psi|^2) \tag{3}$$

and the sound intensity vector $\vec{I}$, which characterizes the means flow of energy:

$$\vec{I} = -\rho\partial_t\Psi\vec{\nabla}\Psi \tag{4}$$

Noting $\vec{J} = \frac{\vec{I}}{c}$, the conservation of energy is given by Eq. (2) along with Eq. (3) and (4):

$$\frac{1}{c}\partial_t E + \vec{\nabla}\cdot\vec{J} = 0 \tag{5}$$

By extension, we still call $\vec{J}$ the sound intensity.

2.2 Sound intensity conservation

In the same way, multiplying Eq. (1) by the gradient $\vec{\nabla}\Psi$ leads to the conservation of sound intensity:

$$\vec{\nabla}\Psi\frac{1}{c^2}\partial_{tt}\Psi - \vec{\nabla}\Psi\Delta\Psi = 0$$

The second member on the left side gives

$$-\vec{\nabla}\Psi\Delta\Psi = -\vec{\nabla}\cdot(\vec{\nabla}\Psi\otimes\vec{\nabla}\Psi) + \vec{\nabla}(\frac{1}{2}|\vec{\nabla}\Psi|^2)$$

where $\otimes$ denotes the outer, or Kronecker, product. The first member gives

$$\vec{\nabla}\Psi\frac{1}{c^2}\partial_{tt}\Psi = \frac{1}{c^2}\partial_t(\partial_t\Psi\vec{\nabla}\Psi) - \frac{1}{c^2}\vec{\nabla}(\frac{1}{2}|\partial_t\Psi|^2)$$

Adding both members, we obtain

$$- \quad \frac{1}{c^2}\partial_t(\partial_t\Psi\vec{\nabla}\Psi) + \vec{\nabla}\cdot(\vec{\nabla}\Psi\otimes\vec{\nabla}\Psi) + \frac{1}{2}\vec{\nabla}(\frac{1}{c^2}|\partial_t\Psi|^2 - |\vec{\nabla}\Psi|^2) = 0 \tag{6}$$

with $\rho(\partial_t\Psi\vec{\nabla}\Psi) = -\vec{I} = -c\vec{J}$.
The conservation of sound intensity is given by Eq. (6) along with Eq. (3) and (4):

$$\frac{1}{c}\partial_t\vec{J} + \vec{\nabla}\cdot\underline{\underline{E}} = 0 \tag{7}$$

where $\underline{\underline{E}}$ is the wave-stress symmetric tensor [15], which does not reduce to the energy density E of equation (3).

2.3 System of coupled equations

Developing the wave-stress tensor, Eq. (5) and Eq. (7) may be written as a system of coupled equations:

$$\begin{gathered}\frac{1}{c}\partial_t E_{tt} + \vec{\nabla}\cdot\vec{J} = 0 \\ \frac{1}{c}\partial_t\vec{J} + \vec{\nabla}\begin{pmatrix} E_{xx} & E_{yx} & E_{zx} \\ E_{xy} & E_{yy} & E_{zy} \\ E_{xz} & E_{yz} & E_{zz}\end{pmatrix} = 0\end{gathered} \tag{8}$$

where the E_{ij} can be expressed in terms of the velocity potential by

$$\begin{aligned} E_{tt} = E &= \frac{\rho}{2}(\frac{1}{c^2}|\partial_t\Psi|^2 + |\vec{\nabla}\Psi|^2) \\ E_{xx} &= \frac{\rho}{2}(\frac{1}{c^2}|\partial_t\Psi|^2 + |\partial_x\Psi|^2 - |\partial_y\Psi|^2 - |\partial_z\Psi|^2) \\ E_{yy} &= \frac{\rho}{2}(\frac{1}{c^2}|\partial_t\Psi|^2 - |\partial_x\Psi|^2 + |\partial_y\Psi|^2 - |\partial_z\Psi|^2) \\ E_{zz} &= \frac{\rho}{2}(\frac{1}{c^2}|\partial_t\Psi|^2 - |\partial_x\Psi|^2 - |\partial_y\Psi|^2 + |\partial_z\Psi|^2) \\ E_{xy} &= \rho\partial_x\Psi\partial_y\Psi \\ E_{xz} &= \rho\partial_x\Psi\partial_z\Psi \\ E_{yz} &= \rho\partial_y\Psi\partial_z\Psi \end{aligned}$$

Note that equations (8) express Emmy Noether (1882-1935)'s famous theorem connecting symmetry with conservation laws.

One can remark that the sound intensity can be noted as $\vec{J} = (J_x, J_y, J_z) = (E_{tx}, E_{ty}, E_{tz})$ where J_x, J_y and J_z are the components of the sound intensity according along the three coordinates. Indeed, the sound intensity vector can be also expressed in terms of the velocity potential by

$$\begin{aligned} E_{tx} &= -\frac{\rho}{c}\partial_t\Psi\partial_x\Psi \\ E_{ty} &= -\frac{\rho}{c}\partial_t\Psi\partial_y\Psi \\ E_{tz} &= -\frac{\rho}{c}\partial_t\Psi\partial_z\Psi \end{aligned}$$

2.4 Stress-energy tensor

We are now able to generalize the energy conservation by combining all the energy quantities E, $\vec{J}$ and $\underline{\underline{E}}$ into a single tensor, the stress-energy tensor:

$$\underline{\underline{T}} = \begin{pmatrix} E & E_{tx} & E_{ty} & E_{tz} \\ E_{tx} & E_{xx} & E_{xy} & E_{xz} \\ E_{ty} & E_{xy} & E_{yy} & E_{yz} \\ E_{tz} & E_{xz} & E_{yz} & E_{zz} \end{pmatrix}$$

which is equivalent to

$$\underline{\underline{T}} = \begin{pmatrix} E & \vec{J}^T \\ \vec{J} & \underline{\underline{E}} \end{pmatrix}$$

with $(\cdot)^T$ the transposed vector.

2.5 Dimensional reduction by integration

Conservation relations between the energy density and sound intensity involve parameters linked to the physical behavior of sound in the medium. Scattering within the volume and on the wall was described by Ollendorf [9] and later by Picault *et al.* [10] under the form of a diffusion coefficient in a diffusion equation. Since the theory of statistical room acoustics was derived by Sabine, researchers have aimed at defining diffusion [17], at characterizing it objectively [18, 19] or subjectively [20]. Here, we complete the system of coupled equations with an energy balance on the walls that naturally introduces acoustic absorption and scattering.

2.5.1 Energy balance on the walls

Starting with the first part of Eq. (8), we consider the propagation of sound in a corridor along the $\vec{x}$ direction with dimensions $l_x \times l_y \times l_z$ where l_x is the length, l_y the width and l_z the height of the corridor. The section of the corridor is given by $S = l_y l_z$. We consider E and J_x constant on the section, J_y is independent of z and J_z is independent of y. We assume strict hypotheses that will be relaxed later, and integrate on the section of the corridor:

$$\begin{aligned} \frac{1}{c}\int_S \partial_t E dS + \int_S \partial_x J_x dS &+ \\ \int_S \partial_y J_y dS &+ \int_S \partial_z J_z dS = 0 \end{aligned} \tag{9}$$

where $dS = dydz$ is an element of the section S, dy and dz are elements of the width and the heigh of the corridor respectively. Resolving Eq. (9) gives a new relation involving wall absorption:

$$\begin{aligned} \frac{1}{c}\partial_t E S + \partial_x J_x S &+ (J_y^+ - J_y^-)l_z \\ &+ (J_z^+ - J_z^-)l_y = 0 \end{aligned} \tag{10}$$

where J_y^+ is the mean sound intensity in the $\vec{y}$ direction next to the wall situated at side $+$. Thus, J_y^+, resp. $-J_y^-$ is the energy flow through the lateral wall $+$, resp. $-$ of the corridor. Additionally, this flow through the wall is proportional to the sound intensity absorbed by the wall:

$$J_y^+ = -J_y^- = J_{abs} \tag{11}$$

We propose to introduce a simple energy balance on the wall. Evidently, the energy flux entering the wall is given by J_y^+ and $|J_y^-|$, the absorbed sound intensities normal to the wall. And the total energy in front of the wall is given by E. As the total energy is non-directional, a quarter of this energy can be considered as entering the wall, as is known from Sabine theory; and a quarter as leaving the wall for symmetrical reasons. In a similar way, half of the normal sound intensity can be considered as entering the wall, and half as leaving it but with a *negative* sign. We then obtains:

$$\begin{aligned} J_{inc} &= \frac{E}{4} + \frac{J}{2} \\ J_{ref} &= \frac{E}{4} - \frac{J}{2} \end{aligned}$$

witch indeed satisfy the energy balance:

$$J_{inc} - J_{ref} = J_{abs}$$

where $J_{abs} = \alpha J_{inc}$ is the sound intensity absorbed by the wall and α is the Sabine absorption coefficient. We have

$$J_{abs} = J = \alpha(\frac{E}{4} + \frac{J}{2})$$

and we recover the relation derived by Jing and Xiang [21]:

$$J = \frac{\alpha}{2(2-\alpha)}E \tag{12}$$

a posteriori justifying our simple energy balance.
We introduce the modified absorption coefficient A:

$$A = \frac{\alpha}{1 - \frac{\alpha}{2}}$$

and Eq. (11) becomes

$$J_y^+ = -J_y^- = J = \frac{A}{4}E$$

likewise for J_z:

$$J_z^+ = -J_z^- = J = \frac{A}{4}E$$

where the coefficient $\frac{1}{4}$ comes from the diffuse field theory [22]. Eq. (10) can now be written as

$$\frac{1}{c}\partial_t ES + \partial_x J_x S + AE\frac{l_y + l_z}{2} = 0 \tag{13}$$

The definition of the mean free path is

$$\lambda = \frac{4V}{S_w} \tag{14}$$

with S_w the total surface area of the walls. The total surface area of a corridor of length l_x, width l_y and height l_z can be developed as $S_w = 2l_x(l_y + l_z) + 2l_y l_z$. Dividing the numerator and the denominator of Eq. (14) by the length l_x of the corridor yields

$$\lambda = \frac{4S}{2(l_y + l_z) + 2\frac{l_y l_z}{l_x}} \tag{15}$$

The corridor is assumed to be long, with $l_y, l_z < 0,1 l_x$. Its width and its height can be neglected in the second term in the denominator of Eq. (15), which becomes

$$\lambda = \frac{2S}{l_y + l_z} \tag{16}$$

Replacing Eq. (16) in Eq. (13), we obtain the following equation:

$$\frac{1}{c}\partial_t E + \partial_x J_x = -\frac{A}{\lambda}E \tag{17}$$

Note that Eq. (17) can easily be generalized to corridors with different absorption coefficient on each walls by simply introducing the mean absorption coefficient.

2.5.2 Momentum balance on the walls

Applying this method to the first component of the second part of Eq. (8) leads to

$$\begin{aligned} \frac{1}{c}\int_S \partial_t J_x dS + \int_S \partial_x E_{xx} dS \quad + \\ \int_S \partial_y E_{xy} dS \quad + \quad \int_S \partial_z E_{xz} dS = 0 \end{aligned} \tag{18}$$

We need not consider the other components as they do not give more information than Eq. (17). We consider J_x and E_{xx} constant on the section, E_{xy} is independent of y and E_{xz} is independent of z. Again, we assume strict hypotheses that will be relaxed later. Integrating Eq. (18) yields

$$\begin{aligned} \frac{1}{c}\partial_t J_x S + \partial_x E_{xx} S \quad + \\ (E^+_{xy} - E^-_{xy}) l_z \quad + \quad (E^+_{xz} - E^-_{xz}) l_y = 0 \end{aligned} \tag{19}$$

where E^+_{xy} is the wave stress next to the wall situated at side $+$. Thus, E^+_{xy}, resp. $-E^-_{xy}$, is the wave stress flow through the lateral wall $+$, resp. $-$ of the corridor.

We postulate that this stress is proportional to the intensity flux scattered by the wall:

$$E^+_{xy} = -E^-_{xy} = M_{scat}$$

where M_{scat} is the sound momentum scattered by the wall. In analogy with the energy balance on the wall (Sec. 2.5.1), we consider that the momentum balance is the sum of two contributions; the intensity flux in the $\vec{x}$ direction (parallel to the wall), and the normal stress. In accordance, a quarter of the intensity flux enters the wall and a quarter leaves the wall, which is coherent to the fact that the intensity J_x is parallel to the wall and must therefore contribute equally to entering and leaving fluxes.

Similarly, half of the stress enters the wall, and half leaves it but with a *negative* sign. We thus obtain, with $M_{xy,ent}$ the entering momentum and $M_{xy,out}$ the outgoing momentum, and with $J = J_x$ as J has only one component:

$$\begin{aligned} M_{xy,ent} &= \frac{E_{xy}}{2} + \frac{J}{4} \\ M_{xy,out} &= -\frac{E_{xy}}{2} + \frac{J}{4} \end{aligned}$$

yielding the following momentum balance:

$$M_{xy,ent} - M_{xy,out} = M_{xy,scat} \tag{20}$$

where $M_{xy,scat} = \beta M_{xy,ent}$, with β the scattering coefficient.

Finally, we have

$$M_{xy,scat} = E_{xy} = \beta(\frac{E_{xy}}{2} + \frac{J}{4})$$

that is

$$E_{xy} = \frac{\beta}{2(2-\beta)}J \tag{21}$$

We introduce the modified scattering coefficient $D = \frac{\beta}{1-\frac{\beta}{2}}$, and Eq. (20) becomes

$$E^+_{xy} = -E^-_{xy} = \frac{D}{4}J$$

likewise for E_{xz}:

$$E^+_{xz} = -E^-_{xz} = \frac{D}{4}J$$

Thus, Eq. (19) reduces to

$$\frac{1}{c}\partial_t JS + \partial_x E_{xx} S + DJ\frac{(l_y + l_z)}{2} = 0$$

from where we obtain, introducing the mean free path of Eq. (16):

$$\frac{1}{c}\partial_t J + \partial_x E_{xx} = -\frac{D}{\lambda}J \tag{22}$$

Eq. (17) and (22) are part of a system of coupled first order partial differential equations. Those equations describe the one-dimensional conservation of the energy density and the sound intensity with absorption and scattering on the walls as function of the modified adsorption and scattering coefficients A and D. The latter accounts for the redistribution of the directions of propagation of energy. In one dimension, the characteristics of absorption and scattering on the walls parallel to the $\vec{x}$ direction are included in the volume equations, whereas the characteristics of the ends walls, perpendicular to the $\vec{x}$ direction, are considered only as boundaries conditions.

As for energy, Eq. (22) can easily be generalized to corridors with different scattering coefficients on each walls, by simply introducing the mean scattering coefficient.

2.6 General equation

Eq. (17) and (22) are similar to the transmission line equations. We exploit this similitude to reduce the system of coupled equations to a single generalized wave equation involving the sound energy density.

We can thereby transform Eq. (17) and (22) as follows:

$$(\frac{1}{c}\partial_t + \frac{A}{\lambda})E = -\partial_x J \tag{23}$$

$$(\frac{1}{c}\partial_t + \frac{D}{\lambda})J = -\partial_x E \tag{24}$$

By derivating Eq. (24) with respect to space, we have

$$(\frac{1}{c}\partial_t + \frac{D}{\lambda})\partial_x J = -\partial_{xx} E$$

Replacing $\partial_x J$ by its value in Eq. (23) yields

$$(\frac{1}{c}\partial_t + \frac{D}{\lambda})(\frac{1}{c}\partial_t + \frac{A}{\lambda})E = \partial_{xx} E$$

Which can be developed in

$$\frac{1}{c^2}\partial_{tt}E - \partial_{xx}E + \frac{A+D}{\lambda c}\partial_t E + \frac{AD}{\lambda^2}E = 0 \tag{25}$$

Eq. (25) is a linear second-order hyperbolic equation called the Telegraph equation. It is constituted of an ordinary wave equation, to which two supplementary terms combine the effect of absorption and scattering. It admits two limiting cases:

- In the *steady state* case, E does not depend on time t, and Eq. (25) reduces to:

$$\partial_{xx}E = \frac{AD}{\lambda^2}E \tag{26}$$

  with solution $E = E_0 e^{-\frac{\sqrt{AD}}{\lambda}|x|}$.

- In the limit of β close to 2, but inferior to it, D tends toward infinity. One can divide Eq. (25) by $\frac{D}{\lambda}$, leading to:

$$\frac{\lambda}{D}(\frac{1}{c^2}\partial_{tt} - \partial_{xx})E + (1 + \frac{A}{D})\frac{1}{c}\partial_t E + \frac{A}{\lambda}E \approx \frac{1}{c}\partial_t E + \frac{A}{\lambda}E = 0$$

  with solution $E = E_0 e^{-\frac{Ac}{\lambda}\cdot t}$. In other words, one recovers Sabine reverberation, albeit with a modified absorption coefficient. However, as J is then very small, the energy remains concentrated around the source.

Note that, when $\alpha = \beta$, Eq. (25) can be exactly factorized into:

$$(\frac{1}{c}\partial_t + \partial_x + \frac{A}{\lambda}) \cdot (\frac{1}{c}\partial_t - \partial_x + \frac{A}{\lambda})E = 0$$

with two travelling sound packets:

$$E^+ = E_0 e^{-\frac{A}{\lambda}ct}\delta(ct - x)$$
$$E^- = E_0 e^{-\frac{A}{\lambda}ct}\delta(ct + x)$$

The time decay is then given by Sabine formula.

2.7 Conditions on the end boundaries

The conditions on the extremities can be written from the energy balance that has been obtained earlier. With respect to the system of coupled equations, the balance gives

$$\vec{J} \cdot \vec{n} = Jn = A_r E$$

where $\vec{n}$ is the vector normal to the wall, and n is equal to ± 1 in one dimension. And A_r is the modified absorption coefficient applied to the boundaries and has already been defined in the literature [21]. We have

$$A_r = \frac{\alpha}{2(2-\alpha)} = \frac{A}{4}$$

It is a Neumann boundary condition. By projecting Eq. (24) on the extremities, we have

$$(\frac{1}{c}\partial_t + \frac{D}{\lambda})Jn = -\partial_x E n$$

We can replace the expression of Jn in Eq. 2.7, we obtain

$$(\frac{1}{c}\partial_t + \frac{D}{\lambda})A_r E = -n\partial_x E$$

for both extremities, and finally

$$n\partial_x E + (\frac{1}{c}\partial_t + \frac{D}{\lambda})A_r E = 0 \tag{27}$$

with $n = +1$ at the "right extremity" (large values of x) and $n = -1$ at the "left extremity" (small values of x). This is a mixed boundary condition. As one can see, the scattering coefficient plays some role in the end boundary conditions.

3 Numerical solving

In this section we present the numerical solving technique that we use to compute the general equation (25). This equation is linear second-order hyperbolic and involve the energy density. Like the transmission lines equations, it is a one-dimensional wave propagation equation. We used this similitude for solving Eq. (25).

3.1 Finite difference time domain simulation

Finite difference time domain (FDTD) methods have been widely used to solve partial differential equations. Yee's 1966 seminal paper [23] first describes the FDTD numerical technique for solving Maxwell's equations. Booteldorren [24] first applied the FDTD method to room acoustics. FDTD technique is a wave based method not commonly used in room acoustics because of its computational cost at high frequencies. For low frequencies problems, FDTD is a fast, direct, time-domain approach that gives locally discretized explicit solutions. In this paper, we use FDTD to solve energetic problem, so we can use larger spatial grids and time steps in comparison with pressure wave equations.

3.2 Schemes

The formulation of the FDTD approximation uses a non staggered grid on energy density components. The energy density is determined at the grid positions $i\Delta x$ and the times $n\Delta t$, with Δx the space discretization step and Δt the time discretization step. Index i marks the space points and index n marks the discrete times.

Schemes have been proposed in the literature for the propagation equation by Booteldorren [24] and Kowalczyk [25]. Savioja [26] simulated real time room acoustics based on those schemes and Navarro Ruiz [27] used a FDTD method based on the diffusion equation to predict sound fields in rooms. On the other hand, Nagel [28] used a revised mesh for the transmission lines equations in case of an one-dimensional electromagnetic wave simulation. Jianhui *et al.* [29] applied a FDTD method to the time domain reflectometry cable length measurement. Mohanty [30] proposed an unconditionally stable difference scheme for a second order linear hyperbolic equation similar to Eq. (25).

Here, we use instead a simplified finite-difference approach which is a centred-time centred-space scheme. The approximations are:

$$\begin{aligned}
\left.\frac{\partial^2 E}{\partial t^2}\right|_x^t &= \frac{E_i^{n+1} - 2E_i^n + E_i^{n-1}}{\Delta t^2} + \mathcal{O}(\Delta t)^2 \\
\left.\frac{\partial^2 E}{\partial x^2}\right|_x^t &= \frac{E_{i+1}^n - 2E_i^n + E_{i-1}^n}{\Delta x^2} + \mathcal{O}(\Delta x)^2 \\
\left.\frac{\partial E}{\partial t}\right|_x^t &= \frac{E_i^{n+1} - E_i^{n-1}}{2\Delta t} + \mathcal{O}(\Delta t)^2
\end{aligned} \tag{28}$$

where $\mathcal{O}(\cdot)$ is the truncation error.

3.3 Discrete general equation

Replacing Eq. (28) in Eq. (25), we have

$$\begin{aligned}
\frac{E_{i+1}^n - 2E_i^n + E_{i-1}^n}{\Delta x^2} &= \frac{E_i^{n+1} - 2E_i^n + E_i^{n-1}}{c^2 \Delta t^2} \\
&+ \frac{E_i^{n+1} - E_i^{n-1}}{2\Delta t} \frac{A + D}{\lambda c} \\
&+ E_i^n \frac{AD}{\lambda^2}
\end{aligned}$$

that is

$$\begin{aligned} E_i^{n+1}(a+1) &= E_i^{n-1}(a-1) + E_i^n(2(1-C_r^2)-b) \\ &+ C_r^2(E_{i+1}^n + E_{i-1}^n) + \mathcal{O}[(\Delta t)^2, (\Delta x)^2] \end{aligned} \tag{29}$$

with $C_r = \frac{c\Delta t}{\Delta x}$ the Courant-Friedrichs-Lewy coefficient, $a = (A+D)\frac{c\Delta t}{2\lambda}$, $b = AD(\frac{c\Delta t}{\lambda})^2$. This equation is a simple explicit form of FDTD. The accuracy of this scheme is second order in time and space.

3.4 Discrete equations on the end boundaries

We model the reflections on the walls. The energy balance on the boundaries gives Eq. (27). The approximations used to this equation are centred space and time:

$$\begin{aligned} \left.\frac{\partial E}{\partial x}\right|_x^t &= \frac{E_{i+1}^n - E_{i-1}^n}{2\Delta x} + \mathcal{O}(\Delta x) \\ \left.\frac{\partial E}{\partial t}\right|_x^t &= \frac{E_i^{n+1} - E_i^{n-1}}{2\Delta t} + \mathcal{O}(\Delta t) \end{aligned}$$

Those approximations are introduced in Eq. (27). The discrete boundaries equation are then used to replace the undefined terms of Eq. (29) on the boundaries. We consider separately the extremities $x = 0$ and $x = nx$ where nx is the length of the model:

$$\begin{aligned} E_1^{n+1}(1+a+A_rC_r) &= E_1^n(2[1-C_r^2(1+\frac{A_rD\Delta x}{\lambda})]-b) \\ &+ 2C_r^2E_2^n + E_1^{n-1}(a-1+A_rC_r) \\ E_{nx}^{n+1}(1+a+A_rC_r) &= E_{nx}^n(2[1-C_r^2(1+\frac{A_rD\Delta x}{\lambda})]-b) \\ &+ 2C_r^2E_{nx-1}^n + E_{nx}^{n-1}(a-1+A_rC_r) \end{aligned} \tag{30}$$

3.5 Initial conditions

Initial conditions corresponds to the source positioned in x by giving $E_i^0 = 0$ except on $i = x$ where it has a given value of $10\log E_x^0 = 100dB$.

3.6 Stability

The maximum size allowed for the simulation steps Δt and Δx to avoid instabilities is now calculated by the Von Neumann analysis. Assuming that the solution of Eq. (29) is given by

$$E_i^n = Z^n e^{j\theta i} \tag{31}$$

where Z can be complex and θ is real, we define the amplification factor as $G = \frac{E_i^{n+1}}{E_i^n}$. The necessary condition for the solution to remain bounded is

$$|G| \leq 1 \tag{32}$$

Substituting Eq. (31) in Eq. (29), we have

$$\begin{aligned} Z^{n+1}e^{j\theta i}(a+1) &= Z^{n-1}e^{j\theta i}(a-1) \\ &+ Z^n e^{j\theta i}(2(1-C_r^2)-b) \\ &+ C_r^2(Z^n e^{j\theta(i+1)} + Z^n e^{j\theta(i-1)}) \end{aligned}$$

with $Z^n(e^{j\theta(i+1)} + e^{j\theta(i-1)}) = 2Z^n\cos(\theta) = 2Z^n(1 - 2\sin^2(\frac{\theta}{2}))$ and dividing by $Z^{n-1}e^{j\theta i}$, we have

$$Z^2(1+a) - Z\epsilon + 1 - a = 0$$

where $\epsilon = -b + 2 - 4C_r^2 sin^2(\frac{\theta}{2})$. This is a second degree equation with solutions depending on the sign of the discriminant $\Delta = \epsilon^2 - 4(1-a^2)$:

- If $\Delta > 0$

$$Z_{\Delta>0} = \frac{\epsilon \pm \sqrt{\Delta}}{2(1+a)}$$

The stability condition Eq. (32) reduces to

$$\left|\frac{\epsilon \pm \sqrt{\Delta}}{2(1+a)}\right| < 1$$

From the triangular inequality,$|\epsilon| + |\sqrt{\Delta}|$ is an upper bound of $|\epsilon + \sqrt{\Delta}|$. With $\Delta > 0$ and $2(1+a) > 0$, a sufficient stability condition is given by

$$\frac{|\epsilon| + \sqrt{\Delta}}{2(1+a)} < 1$$

that is $|\epsilon| < 2$

Replacing by $\epsilon = -b + 2 - 4C_r^2 sin^2(\frac{\Theta}{2})$ and $b = AD(\frac{c\Delta t}{\lambda})^2$, we obtain two conditions:

$$\epsilon < 2, \quad b + 4C_r^2 sin^2(\frac{\theta}{2}) > 0$$

and

$$\epsilon > -2, \quad C_r^2 sin^2(\frac{\theta}{2}) < 1 - \frac{b}{4}$$

The first condition is always satisfied because $b = AD\left(\frac{c\Delta t}{2\lambda}\right)^2 > 0$. The second is obtained by taking the upper bounds of $sin^2(\frac{\theta}{2})$ equal to 1. We have the stability condition for the parameters of the FDTD model:

$$C_r^2(1 + AD(\frac{\Delta x}{2\lambda})^2) < 1 \tag{33}$$

- If $\Delta < 0$

$$Z_{\Delta<0} = \frac{\epsilon \pm i\sqrt{-\Delta}}{2(1+a)}$$

where $i = \sqrt{-1}$. As previously, stability is given by Eq. (32):

$$\left|\frac{\epsilon \pm i\sqrt{-\Delta}}{2(1+a)}\right| < 1$$

As the module of a complex number $z = x + iy$ is given by $|x + iy| = \sqrt{x^2 + y^2}$, we have

$$\frac{\epsilon^2 - \Delta}{4(1+a)^2} < 1$$

Replacing Δ, we have

$$\frac{4(1-a^2)}{4(1+a)^2} = \frac{1-a}{1+a} < 1$$

This condition is always fulfilled since $0 < a < 1$.

We conclude that as long as $\Delta < 0$, the schemes are unconditional stable. If $\Delta > 0$, stability condition given by Eq. (33) must be respected. The stability condition involves the absorption and scattering coefficients, the mean free path and the time and space discretization steps. We study the stability of the model to know the domain of validity of those parameters.

To start with, the space discretization step Δx does not have to be very small as we are studying energy propagation. We set it at $\Delta x = 1m$. Inversely, if the time discretization step is small, results will be precise. We vary the value of Δt between $1.10^{-4}s$ and $1.10^{-2}s$. Then, we set the values for the absorption and scattering coefficients between 0.1 and 0.9, and 0.1 and 1.9 respectively. Finally, we set the free mean path equal to $2m$ and the sound speed at $344m/s$. Table 1 gives the maximum values of Δt for the model to remain stable.

Table 1: Maximum values of Δt to respect the stability condition in function of the model parameters α, β. Other parameters are fixed to $\Delta x = 1m$, $c = 344m/s$ and $\lambda = 2m$.

α	β	$\Delta t(ms)$
0.1	0.1	2.91
	1.1	2.90
	1.9	2.89
0.5	0.1	2.88
	1.1	2.77
	1.9	2.60
0.9	0.1	2.60
	1.1	1.81
	1.9	1.32

One can observe that the stability condition is not sensitive to the variations of the absorption and scattering coefficients, except for large scattering. This is because stability follows a scaling law in accordance with the time and space discretization steps and depends mainly on those parameters.

4 Validation of the models

To assess the general equation, we compute the model with MATLAB. The computation results are first validated by varying the absorption and scattering coefficients. Then, we compare the results with *in situ* measurements. This permits to obtain the coefficients by an adjustment procedure. The results are energy levels presented after time integration for each position of receiver (space decays), and as function of time after source extinction for two receiver positions (time decays).

4.1 Computation results

4.1.1 Model parameters

The FDTD model is calculated for an impulse of $100dB$ through a $32m$ long corridor. The source is situated at $1m$ from the end wall and receivers are positioned every meters form the source. The values of the absorption and scattering coefficients are set from $\alpha = 0.01$ to $\alpha = 0.8$ and from $\beta = 0.01$ to $\beta = 1.5$. The absorption coefficient at both extremities is set to $\alpha_r = \alpha$. The mean free path is set to $\lambda = 2m$, as it corresponds to the mean free path of the corridor measured in Sec. 4.2, and the space and time discretization steps are set to $\Delta x = 1m$, $\Delta t = 1.10^{-3}s$. The speed of sound is $c = 344m/s$.

4.1.2 Space decays

To begin with, Fig. 1 plots the steady-state energy space decays for different values of the absorption and scattering coefficients.

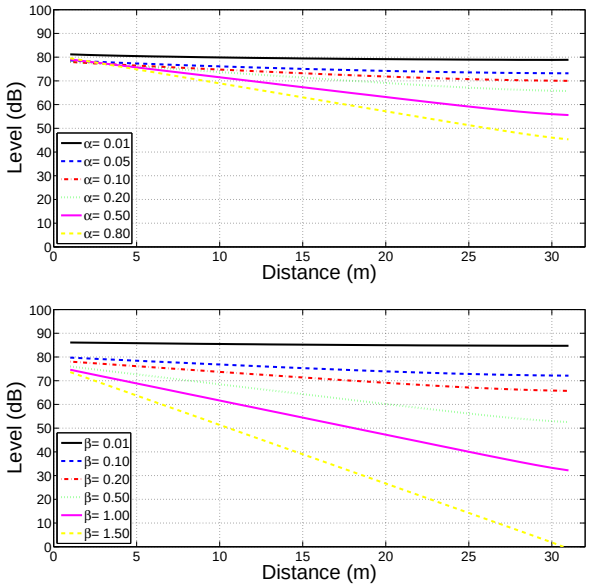

Figure 1: (Colour online) Energy space decays for different values of α (top, with $\beta = 0.2$) and β (bottom, with $\alpha = 0.2$) in a $32m$ long corridor with the source position at $1m$. Parameters are set to $\lambda = 2m$, $\Delta x = 1m$, $\Delta t = 1ms$ and $\alpha_r = \alpha$.

The increase of the slope of the space decays is clearly visible as α or β increase. One can observe that energy clusters around the source for large values of α or β, leading to a steep decrease of energy with distance. Measurement of the decay rates on Fig. 1 gives values varying in the top panel from $0.1dB/m$ for $\alpha = 0.01$ to $1.2dB/m$ for $\alpha = 0.8$; and in the bottom panel, varying from $0.1dB/m$ for $\beta = 0.01$ to $2.5dB/m$ for $\beta = 1.5$. These decay rates correspond to the values expected from Eq. (26).

4.1.3 Time decays

Secondly, Fig. 2 and 3 plot the energy time decays for different values of the absorption and scattering coefficients.

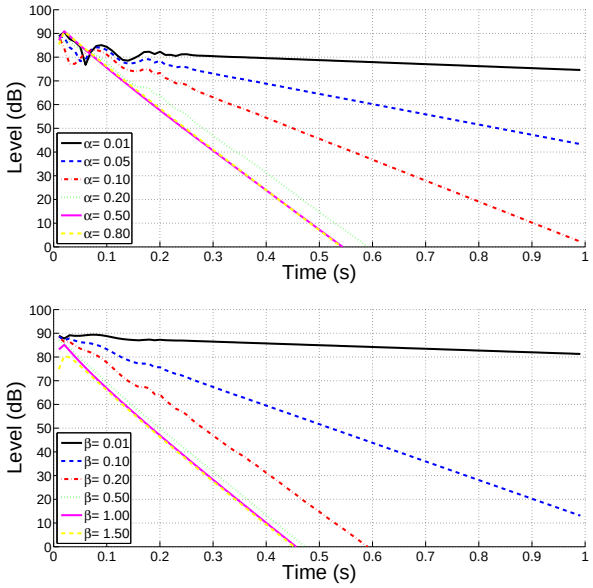

Figure 2: (Colour online) Energy time decays at $4m$ from the source for different values of α (top, with $\beta = 0.2$) and β (bottom, with $\alpha = 0.2$) in a $32m$ long corridor with the source position at $1m$ and the receiver position at $5m$. Parameters are set to $\lambda = 2m$, $\Delta x = 1m$, $\Delta t = 1ms$ and $\alpha_r = \alpha$.

Like the space decays, the slope of the time decays is increasing as α or β increases. The measured decay slopes are in fair agreement with Sabine reverberation $E = E_0 e^{-\frac{Bc}{\lambda} \cdot t}$, where B is equal to the smaller of the two modified coefficients A and D, with a small influence of the other coefficient. Hence, decay rates for $\alpha = 0.01$ in the upper panel ($\beta = 0.2$) and $\beta = 0.01$ in the lower panel ($\alpha = 0.2$) are both equal to 8dB/s; and the steepest decay is reached for $\alpha = 0.2$ in the upper panel, and $beta = 0.2$ in the lower panel, that is in both cases for $\alpha = \beta$. Thus, absorption and scattering are fully equivalent, and the smaller of the two corresponding coefficients pilots the decay.

Note, however, that exchanging α and β does not lead exactly to the same decay curves, as is evident from Fig. 2. This is due to the fact that A_r and D are not exchangeable in the conditions on the end boundaries, that is, in Eq. 27 and 30. Smaller values of α_r or A_r lead to stronger oscillations in the early decay, as is visible from comparing the two panels of Fig. 2.

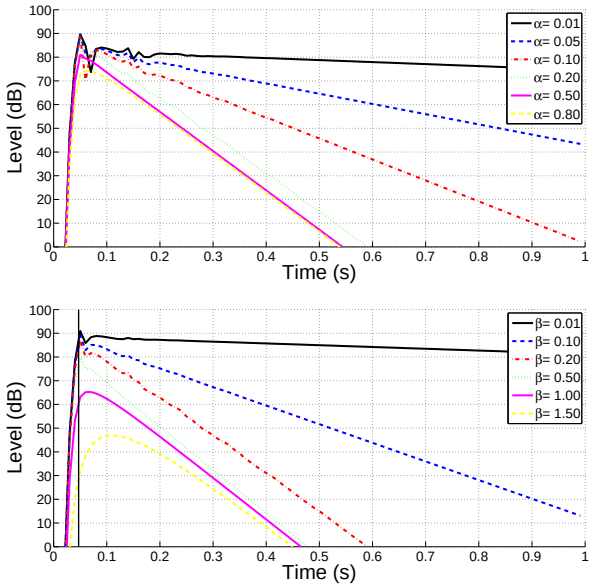

Figure 3: (Colour online) Energy time decays at $16m$ from the source for different values of α (top, with $\beta = 0.2$) and β (bottom, with $\alpha = 0.2$) in a $32m$ long corridor with the source position at $1m$ and the receiver position at $17m$. Parameters are set to $\lambda = 2m$, $\Delta x = 1m$, $\Delta t = 1ms$ and $\alpha_r = \alpha$. The vertical line corresponds to the arrival time of the direct sound (47ms).

At $16m$ from the source, like at $4m$, the time decay slopes increase when α or β increases. Once again, measured decays are in fair agreement with Sabine reverberation obtained for the smaller of the two modified coefficients A and D and are the same as in Fig. 2 for the corresponding values of α and β. Once again, oscillations appear for small values of α_r, but not to the same extend for small values of β. One can also observe that at this distance, the maximum level of the decay decreases when the coefficients increase. Similarly, the arrival time of the maximum increases when the coefficients increase; but the maximum is never attained before the arrival time of the direct sound, marked by a vertical line on the bottom panel of Fig. 3. This was not visible at $4m$ from the source.

4.2 Comparison with measurements

4.2.1 Measurements

The measurements have been made with the help of a *SoundField* ST250 microphone [31]. It is composed of four probes in tetrahedral array from which one can recover the pressure at the central position, and the pressure gradient along the three Cartesian axes. The sound source was an *Outline* GRS omnidirectional speaker constituted of twelve speakers and a *Tannoy* VS10 sub woofer. The source was positioned on the center axis of the corridor at $1m$ from one extremity and at $1.5m$ above the floor. We used a *MOTU*®Traveler sound card and a laptop with *Adobe Audition* software and Aurora plug-in to both send and record the signals. The latter was a $20Hz$ to $20kHz$ $10s$ sweep sine. Signals recorded are post-treated to obtain room impulse responses (IR) by convolution with the inverse sweep. This is known as the most efficient technique to remove harmonic distortions and to increase signal-to-noise ratio [32, 33]. The IR are then used to calculate the sound level by Schroeder's reverse integration [34].

4.2.2 Room characteristics

The room under measurement is a corridor similar to the one-dimensional model. It is $32m$ long, $2.5m$ high and $1.7m$ wide, with a mean free path of $2m$ according to Eq. (16). Several offices are located along the corridor, and some recesses are installed along the corridor, giving more scattering. The corridor ends with a chicane as shows in Fig. 4.

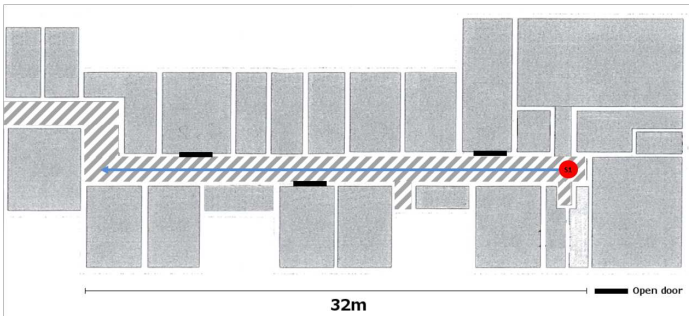

Figure 4: Plan of the corridor under measurement (shaded area). The source $S1$ is shown by a red circle and the axis of measurement by a blue arrow .

The corridor features are carpet on the floor and compact mineral wool on the ceiling. Ceiling is interrupted by ten incised roof windows one meter above a metal grid which is $1.7m$ large and $2m$ long. The walls are constituted of windows and glass doors alternated with metal. Moreover, the corridor is furnished with display stands and cupboards covering one third of the walls and generating scattering.

4.2.3 Adjustment procedure results

Estimations of the absorption and scattering coefficients can be derived from comparison with measurements. We saw above that for values of β larger than α, variations of β do not influence the slope of the time decay. Thus, an iterative procedure has been used to estimate α and β by first assuming β to be large and estimating the absorption coefficient from time decay, then deducing β with the help of the space decay. At each iteration, the previous value of β is used to adjust α so that decay slopes correspond between measurements and numerical simulation, then readjust β from the space decay. The procedure stops when variations are less than 10%, a typical uncertainty in architectural acoustics.

Fig. 5 and 6 plot the time decays (top) that give the absorption coefficients centered on the frequency range $1000Hz$. Then the space decay (bottom) gives the scattering coefficient at $1000Hz$. α is 0.27 for both Fig. 5 and 6. This correspond to a β of 0.37 in both cases, as the bottom panels of Fig. 5 and 6 are the same.

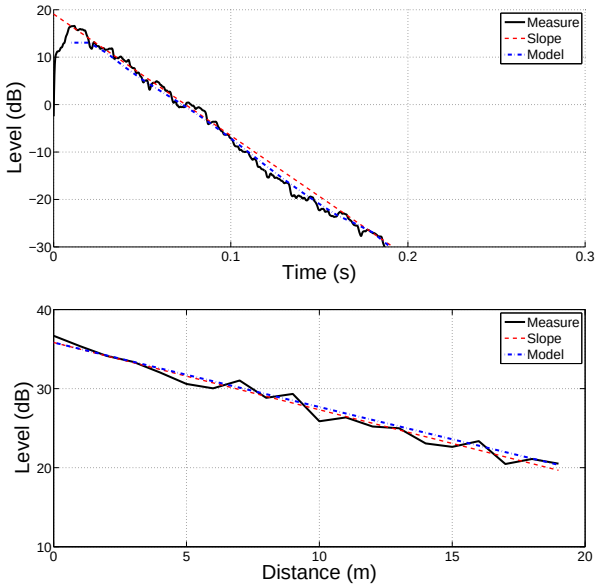

Figure 5: (Colour online) Adjustment of the model by comparison with the time and space decays measured at $4m$ from the source in a corridor of size $1.7m \times 2.5m \times 32m$. $\alpha = 0.27$ and $\beta = 0.37$ at top and bottom panel.

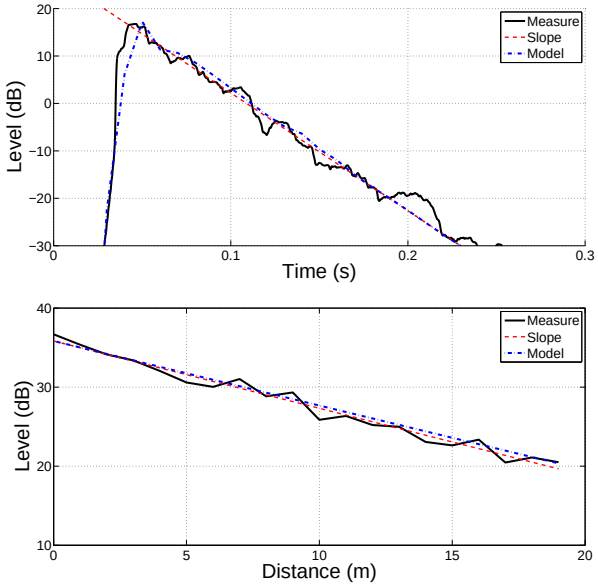

Figure 6: (Colour online) Adjustment of the model by comparison with the time and space decays measured at $16m$ from the source in a corridor of size $1.7m \times 2.5m \times 32m$. $\alpha = 0.27$ and $\beta = 0.37$ at top and bottom panel.

4.2.4 Comparison with Sabine formula

The reverberation times are $Tr = 0.37s$ and $Tr = 0.5s$ at $4m$ and $16m$ from the source respectively. Using Sabine's formula gives a mean of α as

$$\alpha = \frac{0.16V}{TrS}$$

That is, with $V = 136m^3$ and $S = 277.3m^2$, $\alpha = 0.21$ and $\alpha = 0.16$ at $4m$ and $16m$ respectively, compared to $\alpha = 0.27$ obtained previously.

5 Discussion

5.1 Relaxing integration hypotheses

Sec. 2.5.1 and 2.5.2 requested strict mathematical hypotheses for integrating the conservation equations in order to reduce the dimension. Here, we analyze those hypotheses and relax them when possible.

The hypotheses are:

- E and J_x are constant on the section S of the corridor, but J_y and J_z are only independent of z and y respectively
- J_x and E_{xx} are constant on the section, and E_{xy} and E_{xz} are independent of z and y respectively.

In order to relax the hypotheses, we need to look back at Eq. (9) and (18) where the integration is carried out. As E, E_{xx} and J_x are integrated on the section in both equations, we are in fact only considering the mean value of these quantities. Therefore, they may vary across the section; the integrals thus become, with the upper line indicating mean values:

$$\begin{aligned} \int_S E dx &= \overline{E} S \\ \int_S E_{xx} dx &= \overline{E_{xx}} S \\ \int_S J_x dx &= \overline{J_x} S \end{aligned}$$

J_y and E_{xy} were considered as independent of z only; for the same reason, their integrals on the two sidewalls at y^+ and y^- can be replaced by $\overline{J_y^+} l_z$ and $\overline{J_y^-} l_z$, and $\overline{E_{xy}^+} l_z$ and $\overline{E_{xy}^-} l_z$. The same applies to J_z and E_{xz}, the integrals of which on the sidewalls z^+ and z^- are replaced by $\overline{J_z^+} l_y$ and $\overline{J_z^-} l_y$, and $\overline{E_{xz}^+} l_y$ and $\overline{E_{xz}^-} l_y$.

Further hypotheses considered $J_y^+ = J_y^- = J_{abs}$, and $E_{xy}^+ = E_{xy}^- = M_{scat}$, and similar hypotheses for J_z and E_{xz}. Indeed, this last group of hypotheses can easily be relaxed by considering balances on each wall separately - but now with mean values for the E_s and J_s - with different absorption and scattering coefficients, then aggregate the results to obtain the *mean* absorption and scattering coefficients $\overline{A}$ and $\overline{D}$ on the four walls. As a consequence, Eq. (17) and (22) can be rewritten as:

$$\begin{aligned} \frac{1}{c} \partial_t \overline{E} + \partial_x \overline{J_x} &= -\frac{\overline{A}}{\lambda} \overline{E} \\ \frac{1}{c} \partial_t \overline{J} + \partial_x \overline{E_{xx}} &= -\frac{\overline{D}}{\lambda} \overline{J} \end{aligned}$$

Note that the product of mean values is a consequence of the heuristic definition of absorption and scattering coefficients by Eq. (12) and (21), with mean values for E and J.

Last but not least, as integration is only carried out on a cross section of the corridor, all values, *including those of the absorption and scattering coefficients*, may vary with position along the corridor. Therefore, the model intrinsically allows position varying absorption and scattering coefficients. However, the general equation of Sect. 2.6 must be modified accordingly.

5.2 Domain of validity of absorption and scattering coefficients

The reader may have been intrigued by the range of values for the scattering coefficient β in Fig. 1, 2, and 3, where β can be larger than 1. In fact, whereas an absorption coefficient is limited to values ranging from 0 to 1, as no energy can be negative, and no wall can absorb more energy than what impinges on it, there is no limit for the modified scattering coefficient: from Eq. (21), a value of $D = 0$ simply means that $E_{xy} = 0$ or $E_{xz} = 0$, just as a value of $D = +\infty$ means $J_x = 0$. No energy is at stakes in the process, only directional redistribution of the acoustic intensity.

However, absorption and scattering coefficients play similar rôles in Eq. (25). In fact, they can be exchanged without any modification of the equation. This behaviour is reminiscent of coupled rooms [6], where E and J would be equivalent to the energy of two rooms. This analogy can be used to derive an approximative analytical solution to equation (25):

$$E = E_A e^{-\frac{A_c}{\lambda} \cdot t} + E_D e^{-\frac{D_c}{\lambda} \cdot t}$$

The slower decay of the two will pilot the behavior at long times, whereas the two interfere at short times in accordance to the oscillations observed in Fig. 2 and 3. Note that the spatial derivatives in Eq. (23) and (24) introduce the coupling, leading to deviations in the decays rates of the two terms of the approximate analytical solution, as visible in Fig. 2 and 3.

5.3 Adjustment procedure

The adjustment gives quite good results, as shown by Fig. 5 and 6. The difference with the Sabine formula is due to the non-diffuse field in the corridor. Sabine formula consider the energy to be homogeneous but we show that the reverberation in a disproportionate space is given by the local volume (the section) and that diffusion concentrates energy around the source. Therefore, energy varies along the corridor, and reverberation can be different at different positions, even though differences are minimized by the diffusion process. Indeed, if the reverberation time was significantly longer at some given position, the local energy difference with the neighbouring positions would increase with time; diffusion, that is, Eq. (24), will then reduce the difference by increasing the energy flow, thus levelling reverberation times around the given position.

5.4 Time of arrival of the direct sound

Fig. 2 and 3 show different times of arrival of the energy. Fig. 2 was calculated at $4m$ from the source and Fig. 3 at $16m$, which gives times of arrival of the direct sound of resp. $12ms$ and $47ms$. The Figure shows that part of the energy is coming earlier than the time of propagation: this is due to the discretization scheme of Sect. 3, which allows small amounts of precursor signals. However, the maximum does correspond to the expected time of arrival for low scattering values in the lower panel of Fig. 3. The time of arrival of the energy depends on the absorption and scattering coefficients, with higher values of the scattering coefficient delaying more the energy.

6 Conclusion

In this paper, we have shown that the conservation of energy in a given volume consists of two equations: the conservation of the total energy; and the conservation of sound intensity. The two equations combine in a single tensor equation, the conservation of the stress-energy tensor.

In one or two dimensions, absorption and scattering on the walls modify these conservation equations. We solved this system of two equations in the case of a one-dimensional system by combining them into a single Telegraph equation involving energy only, and by using of a finite difference scheme. We showed that our scheme is stable and then compared simulations to actual measurements in a corridor. The comparison permits adjusting the absorption and scattering coefficients to obtain good agreement, leading to measurement methods for the two coefficients.

Further, systematic variations of the absorption or scattering coefficient while retaining the other coefficient constant, showed that the two coefficients play similar rôles as is visible in the Telegraph equation; however, only the smaller of the two absorption and scattering coefficients

pilots the time decay rate. Thus, the two coefficients can be evaluated sequentially from an initial guess: the smaller coefficient from the time decay curves; and the larger from the space decay curve. It should be noted that adjustment is local, that is, the procedure permits the evaluation of locally varying absorption and scattering coefficients. On the other hand, increased scattering leads to accumulation of energy around the source, and to a rapid diminution of energy with distance from the source.

In future papers, we shall compare our model to Ollendorf and Picaut's analytical model, and investigate the two-dimensional case, including again comparison with measurements.

Acknowledgement

This work was carried out under a CIFRE convention (n° 2012/1184) between Impédance S.A.S. and Université Pierre et Marie Curie (Institut Jean le Rond d'Alembert), thanks to a grant from ANRT.

References

[1] B.-I. Dalenbäck, "Engineering principles and techniques in room acoustics prediction," in *Baltic-Nordic Acoustics Meeting (BNAM)*, (Bergin, Norway), 2010.

[2] T. J. Cox, "The optimization of profiled diffusers," *J. Acoust. Soc. Am.*, vol. 97, no. 5, pp. 2928–2936, 1995.

[3] A. James, B. I. Dalenback, and A. Naqvi, "Computer modelling with CATT-Acoustic - Theory and practice of diffuse reflection and array modeling," 2001.

[4] M. Vorlander, "International round robin on room acoustical computer simulations," *International Congress on Acoustics 15th*, 1995.

[5] B. Katz, "International Round Robin on Room Acoustical Impulse Response Analysis Software 2004," *Acoustical Society of America ARLO 5(4), October 2004*, 2004.

[6] H. Kuttruff, *Room acoustics*. London & New York: Spon Press/Taylor & Francis, 2009.

[7] T. H. Lewers and J. S. Anderson, "Some acoustical properties of St Paul's Cathedral, London," *Journal of Sound and Vibration*, vol. 92, no. 2, pp. 285–297, 1984.

[8] M. Hodgson, "When is Diffuse-Field Theory Applicable?," *Appl. Ac.*, vol. 49, no. 3, pp. 191–201, 1996.

[9] F. Ollendorff, "Statistical room acoustics as a problem of diffusion, a proposal," *Acustica*, vol. 21, pp. 236–245, 1969.

[10] J. Picaut, L. Simon, and J. D. Polack, "A mathematical model of diffuse sound field based on a diffusion equation," *Acta Acust united Ac*, vol. 83, no. 4, pp. 614–621, 1997.

[11] C. Foy, V. Valeau, A. Billon, J. Picaut, and A. Sakout, "An Empirical Diffusion Model for Acoustic Prediction in Rooms with Mixed Diffuse and Specular Reflections," *Acta Acust united Ac*, vol. 95, no. 1, pp. 97–105, 2009.

[12] J.-D. Polack, "Sound fields in rooms: an introduction to reverberation theory," *Acoustic Quality of Concert Halls. State of the Art and Research Trends, Spanish Acoust. Soc.*, pp. 27–61, 1995.

[13] J. Picaut, I. Schmich, J. Defrance, P. Woloszyn, A. Barlet, and F. Chartier, "Effets de la réflexion diffuse des façades sur la propagation acoustique et sur la représentation de l'environnement sonore en milieu urbain. 4ème assises de la qualité l'environnement sonore," *Acoustique et Techniques*, no. 39, 2004.

[14] P. M. Morse and H. Feshbach, *Method of Theoretical Physics*. Mc Graw-Hill Book Company, 1953.

[15] P. M. Morse and K. U. Ingard, *Theoretical Acoustics*. Mc Graw-Hill Book Company, 1968.

[16] J.-J. Embrechts, "Modelisation des reflexions diffuses en acoustique des salles : etat de la question," in *6ème Congrès Français d'Acoustique (CFA)*, 2002.

[17] E. Mommertz, "Determination of scattering coefficients from the reflection directivity of architectural surfaces," *Appl. Ac.*, vol. 60, pp. 201–203, 2000.

[18] J. H. Rindel and J. Y. Jeon, "The new field method for measurement of the scattering coefficient," *communication personnelle et notes,*, 2003.

[19] T. Sakuma, Y. Kosaka, L. Geetere, and M. Vorlander, "Relationship between the scattering coefficients determined with coherent averaging and with directivity correlation," *Acta Acust united Ac*, vol. 95, no. 4, pp. 669–677, 2009.

[20] J. K. Ryu and J. Y. Jeon, "Subjective and objective evaluations of a scattered sound field in a scale model opera house," *J. Acoust. Soc. Am.*, vol. 124, no. 3, pp. 1538–1549, 2008.

[21] Y. Jing and N. Xiang, "On boundary conditions for the diffusion equation in room acoustic prediction: theory, simulations, and experiments," *J. Acoust. Soc. Am.*, vol. 123, no. 1, pp. 145–153, 2008.

[22] V. Valeau, J. Picaut, and M. Hodgson, "On the use of a diffusion equation for room-acoustic prediction," *J. Acoust. Soc. Am.*, vol. 119, no. 3, pp. 1504–1513, 2006.

[23] K. S. Yee, "Numerical solution of boundary value problems involving Maxwell's equations in isotropic media," *IEEE Transactions on antennas and propagation*, 1966.

[24] D. Botteldooren, "Finite-difference time-domain simulation of low-frequency room acoustic problems," *J. Acoust. Soc. Am.*, vol. 98, no. 6, pp. 3302–3308, 1995.

[25] K. Kowalczyk, *Boundary and medium modelling using compact finite difference schemes in simulations of room acoustics for audio and architectural design applications*. PhD thesis, School of Electronics, Electrical Engineering and Computer Science, Belfast, 2008.

[26] L. Savioja, "Real-time 3d finite-difference time-domain simulation of low-and mid-frequency room acoustics," in *13th Int. Conf on Digital Audio Effects (DAFx-10)*, (Graz, Austria), 2010.

[27] J. M. Navarro Ruiz, J. Escolano, and J. J. López, "Implementation and evaluation of a diffusion equation model based on finite difference schemes for sound field prediction in rooms," *Appl. Ac.*, vol. 73, no. 6-7, pp. 659–665, 2012.

[28] J. R. Nagel, "The Finite-Difference Time-Domain (FDTD) Algorithm," tech. rep., Department of Electrical And Computer Engineering, University of Utah, 2010.

[29] S. Jianhui, L. Yanju, and Y. Yang, "Numerical analysis of transmission line telegraph equation based on FDTD method," *JCIT*, vol. 7, no. 20, pp. 258–265, 2012.

[30] R. Mohanty, "An unconditionally stable finite difference formula for a linear second order one space dimensional hyperbolic equation with variable coefficients," *App. Math. Comput.*, vol. 165, no. 1, pp. 229–236, 2005.

[31] J. P. Espitia Hurtado, H. Dujourdy, and J. D. Polack, "Caractérisation expérimentale du microphone SoundField ST250 pour la mesure de la diffusivité du champ sonore," in *12ème Congrès Français d'Acoustique (CFA)*, (Poitiers, France), pp. 795–801, 2014.

[32] P. Fausti and A. Farina, "Acoustic measurements in opera houses: comparison between different techniques and equipment," *Journal of Sound and Vibration*, vol. 232, no. 1, pp. 213–229, 2000.

[33] S. Muller and P. Massarani, "Transfer-function measurement with sweeps," *J. Audio Eng. Soc.*, vol. 49, no. 6, pp. 443–471, 2001.

[34] M. R. Schroeder, "New method for measuring reverberation time," *J. Acoust. Soc. Am.*, vol. 37, pp. 409–412, 1965.